Two-gap superconductivity and topological surface states in TaOsSi

C. Q. Xu,[1,2] B. Li,[3] J. J. Feng,[1] W. H. Jiao,[4] Y. K. Li,[5] S. W. Liu,[1] Y. X. Zhou,[6] R. Sankar,[7] Nikolai D. Zhigadlo,[8,9] H. B. Wang,[2] Z. D. Han,[2] B. Qian,[2] W. Ye,[1,*] W. Zhou,[2,†] T. Shiroka,[10] Pabitra K. Biswas,[11] Xiaofeng Xu,[2] and Z. X. Shi[1,‡]

[1]*School of Physics and Key Laboratory of MEMS of the Ministry of Education, Southeast University, Nanjing 211189, China*
[2]*Department of Physics, Changshu Institute of Technology, Changshu 215500, China*
[3]*Information Physics Research Center, Nanjing University of Posts and Telecommunications, Nanjing 210023, China*
[4]*Department of Physics, Zhejiang University of Science and Technology, Hangzhou 310023, China*
[5]*Department of Physics and Hangzhou Key Laboratory of Quantum Matters, Hangzhou Normal University, Hangzhou 310036, China*
[6]*Department of Physics, Zhejiang University, Hangzhou 310007, China*
[7]*Institute of Physics, Academia Sinica, Nankang, Taipei, 11529, Taiwan*
[8]*Department of Chemistry and Biochemistry, University of Bern, CH-3012 Bern, Switzerland*
[9]*CrystMat Company, CH-8046 Zurich, Switzerland*
[10]*Laboratorium für Festkörperphysik, ETH Hönggerberg, Zürich, CH-8093, Switzerland*
[11]*ISIS Pulsed Neutron and Muon Source, STFC Rutherford Appleton Laboratory, Harwell Campus, Didcot, Oxfordshire OX11 0QX, United Kingdom*

(Received 13 June 2019; revised manuscript received 2 September 2019; published 4 October 2019)

The occurrence of superconductivity in topological materials is considered as a promising route for realizing topological superconductors, a platform able to host the long-sought Majorana fermions in condensed matter. In this work, by using electrical transport and heat-capacity measurements, as well as first-principles band-structure calculations, we investigate the physical properties of TaOsSi, a superconductor with $T_c \approx 5.8$ K. The behavior of both its upper critical field and low-temperature heat-capacity suggest the existence of two superconducting gaps. More strikingly, first-principles calculations reveal gapless topological surface states in the present material. The evolution of the electrical resistivity with pressure (up to 50 GPa) was also investigated, and a "V-shaped" diagram of T_c vs P was found. Overall, our data suggest that TaOsSi is a new system where multiband superconductivity and topological surface states coexist and, hence, it may serve as a possible candidate in the search for topological superconductivity.

DOI: 10.1103/PhysRevB.100.134503

I. INTRODUCTION

Unlike the common Dirac fermions, Majorana fermions are exotic particles which represent their own antiparticle. Originally investigated within the scope of particle physics, due to possible uses in quantum computation [1–6], they have been facing an increasing interest also by condensed-matter physicists. In condensed matter, Majorana fermions may exist as emergent collective excitations of electrons, typically observed at the boundaries of topological superconductors or in some spin-liquid systems [1]. Two key conditions should be satisfied in order to realize Majorana fermions from collective excitations [1]: (1) compliance with the Dirac equation, and (2) self-conjugation. Topological superconductors, hosting not only a fully gapped superconducting bulk state, but also a gapless surface state, are natural systems for observing the Majorana bound states. Indeed, here the particle-hole symmetry, resulting from the superposition of electron and hole excitations in a superconductor, jointly with the topological gapless boundary excitations, make such systems ideal candidates [1,3].

Currently, two possible realizations of topological superconductors are envisioned, including either the spin-triplet (i.e., odd-parity) pairing superconductors, or the superconducting topological surface states induced by the proximity effect from an s-wave superconductor [1,3,7–9]. As for the first proposal, if one excludes the controversial Sr_2RuO_4 [10–13], the doped topological insulator $Cu_xBi_2Se_3$ [14–16], and some noncentrosymmetric superconductors [17,18], the currently known spin-triplet superconductors are rather scarce. As for the second proposal, the inhomogeneity induced by doping usually hinders the realization of Majorana bound states at the vortex cores. Currently, due to the burgeoning discovery of topological semimetals, researchers have been gradually shifting their attention to topological systems that simultaneously exhibit also intrinsic superconductivity. Such peculiar compounds include, e.g., $PbTaSe_2$ [19,20], β-$PdBi_2$ [21,22], and RPtBi (R = rare earth) [23–25].

Recently, two new superconductors, TaOsSi ($T_c \sim 5.5$ K) and NbOsSi ($T_c \sim 3.5$ K), have been discovered [26]. Due to the presence of heavy transition-metal elements, such as Ta and Os, and the ensuing spin-orbit coupling (SOC) effects on the band structure, TaOsSi represents a potentially interesting material. Since to date its superconducting properties have

*yewei@seu.edu.cn
†wei.zhou@cslg.edu.cn
‡zxshi@seu.edu.cn

never been studied, here we attempt a detailed investigation of its electronic properties, upper critical field, and superconducting gap, via electrical transport and heat-capacity measurements, as well as via first-principles band-structure calculations. Surprisingly, the experimental results indicate that TaOsSi is a two-gap superconductor, while calculations suggest the occurrence of topological surface states. The simultaneous presence of superconductivity and topological effects makes TaOsSi a possible candidate in the search for topological superconductivity and Majorana fermions.

II. EXPERIMENTAL DETAILS

Polycrystalline TaOsSi specimens were synthesized via the arc-melting method. Tantalum pellets, osmium ingots, and silicon pieces, all 99.99% pure (from Alfa Aesar) were used as starting materials. Once prepared in a 1 : 1 : 1 molar ratio, the reagents were inserted into an arc furnace, which was purged multiple times and eventually filled with pure argon. To ensure phase homogeneity, the as-cast ingot was remelted more than ten times. The final ingot was sealed under vacuum in a quartz tube and then annealed at 1273 K for about nine days. The room-temperature structure was determined via x-ray diffraction (XRD) by using a Rigaku diffractometer with Cu Kα radiation and a graphite monochromator. The heat capacity and electrical resistivity were measured by means of a physical property measurement system (PPMS-9T), while the magnetization was measured by using a magnetic property measurement system (MPMS-7T), both from Quantum Design. To determine the electrical resistivity under applied-pressure conditions, we employed a diamond-anvil cell. Here, pressures up to 50 GPa could be achieved by using anvils 300 μm in diameter and sodium chloride as a pressure-transmitting medium. The pressure value at room temperature was measured by monitoring the shift of the fluorescence line of a ruby sphere.

The electronic band structures were computed by using the full-potential linearized augmented plane wave (FP–LAPW) method, as implemented in the WIEN2K code [27]. Relativistic and spin-orbit coupling (SOC) effects were included in all the calculations. The generalized gradient approximation (GGA) [28] was used to calculate the exchange-correlation potential. A muffin-tin potential with a radius of 2.5 a.u. was chosen for the Ta and Os atoms, and of 1.87 a.u. for the Si atoms. The plane-wave cutoff was defined by the condition $rk_{\max} = 7.0$, with r being the minimum LAPW sphere radius and $k_{\max}$ being the plane-wave-vector cutoff. The self-consistent band-structure calculation was performed over a mesh of $10 \times 10 \times 9k$ points. To obtain the Fermi-surface properties, a tight-binding model based on maximally localized Wannier functions [29,30] was constructed. This could reproduce the band structure of the bulk, including the spin-orbit coupling with the Ta d, Os s and d, and Si p orbitals. The band structure and the Fermi surface were calculated on a dense mesh of $24 \times 39 \times 20$ k points in the first Brillouin zone.

III. RESULTS

TaOsSi crystallizes in the TiNiSi orthorhombic structure with space group *Pnma* (No. 62, centrosymmetric). As shown in Fig. 1, powder x-ray diffraction measurements followed by Rietveld refinements allowed us to determine the TaOsSi lattice parameters: $a = 6.26(5)$ Å, $b = 3.89(3)$ Å, and $c = 7.25(9)$ Å. The almost-zero residuals indicate a good sample quality and the lack of spurious phases.

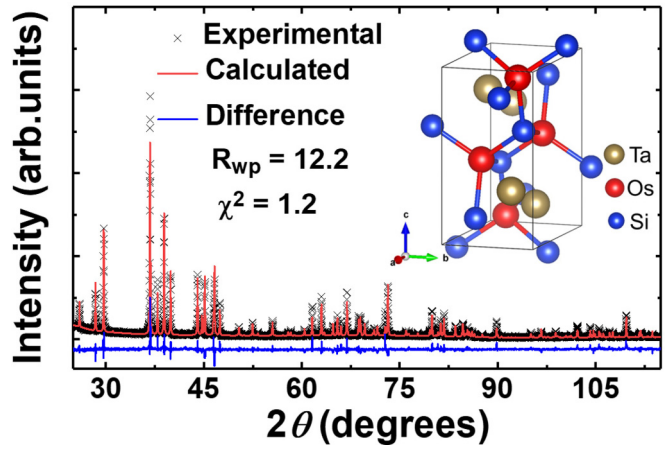

FIG. 1. Powder XRD pattern and Rietveld refinement for TaOsSi. The blue line at the bottom indicates the residuals. The inset shows the orthorhombic crystal structure of TaOsSi.

The temperature-dependent resistivity $\rho(T)$, magnetic susceptibility $\chi(T)$, and heat capacity C/T of TaOsSi are shown in Fig. 2. Starting from 300 K, the sample is first metallic then, once cooled below $T_c \sim 5.8$ K, it enters the superconducting phase. The residual-resistivity ratio RRR ($\rho_{300\mathrm{K}}/\rho_{0\mathrm{K}}$) is circa 5.9. As shown in the inset of Fig. 2(a), the low-temperature resistivity can be nicely fit with a power-law function $\rho = \rho_0 + AT^2$, with $A = 9.66 \times 10^{-4}$ $\mu\Omega$ cm K^{-2}. The quadratic temperature dependence reflects the scattering of electrons off each other in the presence of a crystal lattice and ultimately suggests a Fermi-liquid behavior [31].

The bulk superconductivity of TaOsSi was confirmed by a perfect diamagnetic response and a large specific-heat jump at T_c, as shown in Figs. 2(b) and 2(c). The normal-state heat capacity was fit by $C/T = \gamma_n + \beta T^2 + \delta T^4$, the first term being related to electronic contributions and the other two to phononic contributions. The fit yields a Sommerfeld constant $\gamma_n = 8.52$ mJ mol^{-1} K^{-2}, $\beta = 0.027$ mJ mol^{-1} K^{-4}, and $\delta = 0.0015$ mJ mol^{-1} K^{-6}. From β we determine a Debye temperature of 595 K, 25% higher than the calculated one reported in Ref. [32]. The Kadowaki-Woods ratio (KWR) is $A/\gamma^2 \approx 13.3$ $\mu\Omega$ cm (mol^{-1} K^{-1} J)^2, a value very close to those found in strongly correlated electron systems, such as heavy fermions [33], or in some recently discovered topological semimetals [34]. This suggests that electron-electron correlation effects may not be neglected in TaOsSi.

The temperature-dependent resistivity measurements at different applied fields are shown in Fig. 3(a). As the field increases, the superconducting transition is gradually suppressed to lower temperatures. By locating the points where ρ drops to 90% (or 50%) of its normal-state value ρ_n just above T_c, we can determine the temperature dependence of the upper critical field H_{c2}, shown in Fig. 3(b). Apparently, both $H_{c2}(T)$ curves, extracted using the 90% or the 50% criterion, exhibit an upward curvature. A similar H_{c2}-T diagram has

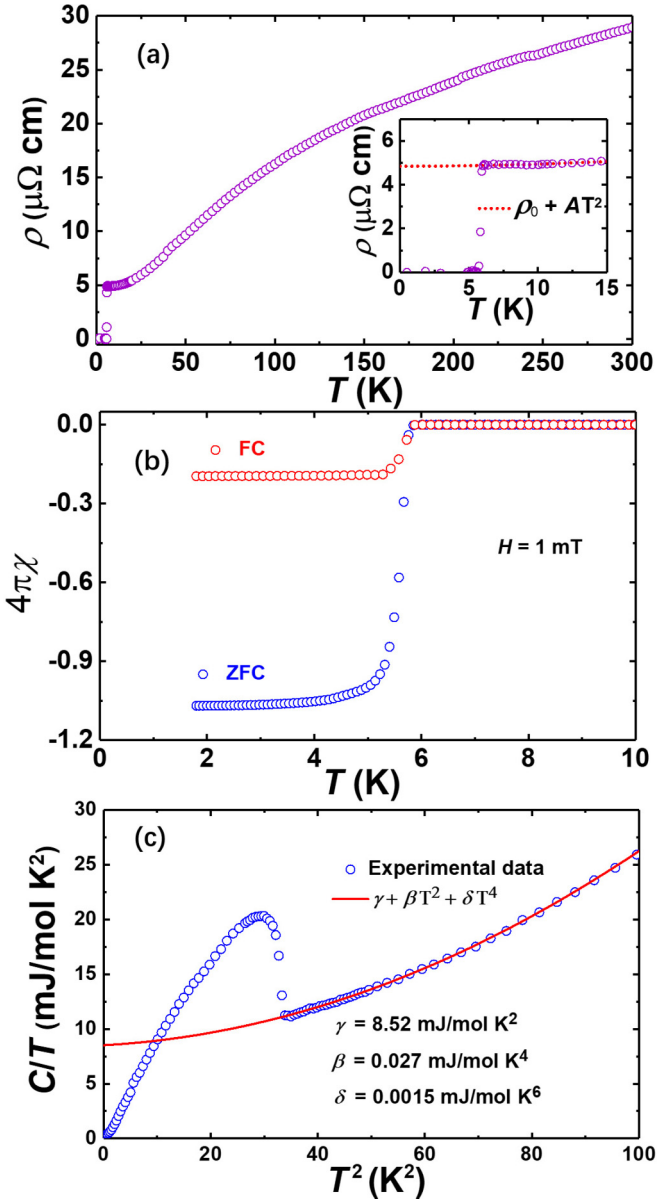

FIG. 2. (a) Temperature dependence of resistivity. Inset: At low temperature (above T_c), $\rho(T)$ is proportional to T^2, a behavior compatible with Fermi-liquid theory. (b) Temperature dependence of magnetic susceptibility for a zero-field cooling (ZFC) and a field cooling (FC) process. (c) Temperature dependence of heat capacity, plotted as C/T versus T^2. The red solid line is a fit based on $C/T = \gamma_n + \beta T^2 + \delta T^4$.

also been observed in MgB_2 [35] and in some unconventional superconductors [36–38], and most likely suggest a two-band superconductivity in TaOsSi. The two-band model for H_{c2} can be expressed as [39]

$$1 = a_0[\ln t + U(h)][\ln t + U(\eta h)] + a_1[\ln t + U(h)] + a_2[\ln t + U(\eta h)], \quad (1)$$

where a_0, a_1, a_2 are determined by the matrix

$$\begin{pmatrix} \lambda_{11} & \lambda_{12} \\ \lambda_{21} & \lambda_{22} \end{pmatrix},$$

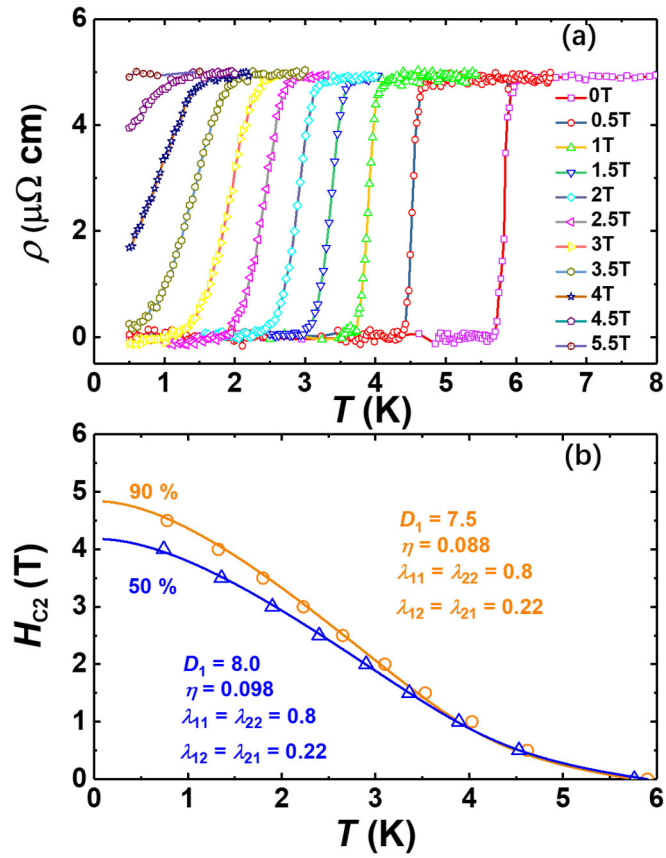

FIG. 3. (a) Temperature dependence of resistivity in different applied magnetic fields. (b) Temperature dependence of the upper critical field, as obtained by the 90% and the 50% criteria (see main text). Solid lines represent fits based on a two-band model.

$h = \frac{H_{c2}D_1}{2\phi_0 T}$, $\eta = \frac{D_2}{D1}$, and $U(x) = \psi(x + \frac{1}{2}) - \psi(\frac{1}{2})$, with $\psi(x)$ being the digamma function. Here, the diagonal (off-diagonal) λ terms express the intraband (interband) coupling constants, while D_1, D_2 denote the diffusivity of each band. As seen in Fig. 3(b), the two-band theory can fit the experimental data overall within the error bars, and the resultant parameters are given in the figure. The best fits of the experimental $H_{c2}(T)$ data give $\eta = 0.088$ when employing the 90% criterion and $\eta = 0.098$ with the threshold set at 50%. Apparently, $H_{c2}(0)$ does not exceed the Pauli paramagnetic limit ($\mu_0 H_{\text{Pauli}} = 1.85T_c \approx 10.7$ T), the field where the magnetization polarization energy equals the condensation energy of the superconducting state (with fields above H_{Pauli} breaking the Cooper-pair singlets).

To confirm the two-band superconductivity of TaOsSi, we further analyzed its low-temperature heat capacity. The temperature dependence of ΔC, shown in Fig. 4(a), was modeled by means of different gap functions (see, e.g., Refs. [40,41]). In the BCS theory, the zero-field electronic heat capacity C_{es} in the superconducting state is derived from the entropy S_{es} by using the relation $C_{es} = T(\partial S/\partial T)$, where [40]

$$S_{es} = \frac{3\gamma_n}{k_B \pi^3} \int_0^{2\pi} \int_0^{\infty} [(1-f)\ln(1-f) + f \ln f] d\varepsilon \, d\phi. \quad (2)$$

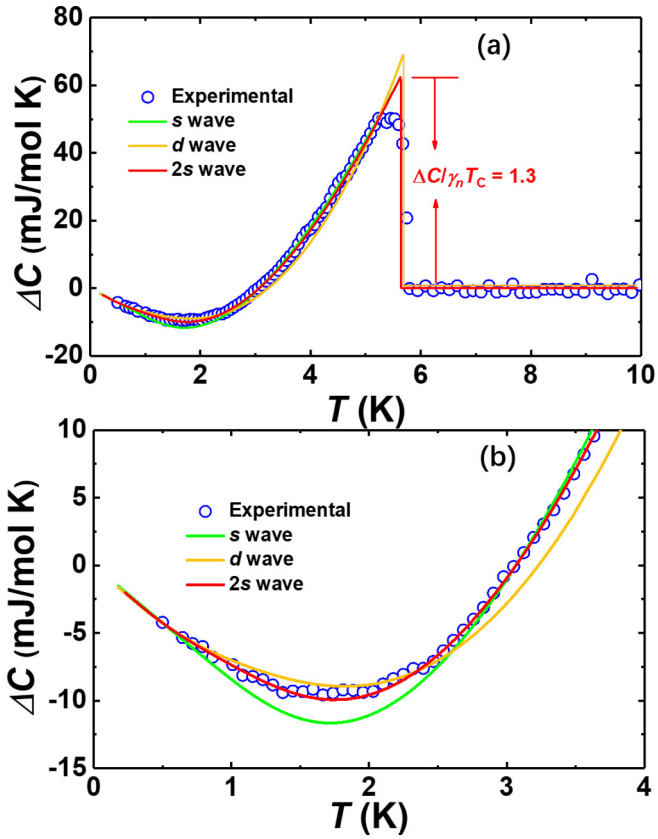

FIG. 4. (a) ΔC versus T. Here $\Delta C = C - C_n$, with C_n being the heat capacity in the normal state. (b) The lower panel shows an enlarged view of the low-T region, where $\Delta C(T)$ is fit by using different gap-symmetry functions.

Here, γ_n is the normal-state Sommerfeld coefficient, $f = 1/(1+\exp^{E/k_BT})$ is the Fermi distribution [with $E = [\varepsilon^2 + \Delta^2(\phi)]^{1/2}$ being the quasiparticle occupation number), and $\Delta(\phi)$ is the angular dependence of the gap function. For a conventional s-wave superconductor, $\Delta(\phi)$ is a constant, while for a d-wave superconductor $\Delta(\phi) = \alpha\Delta(T)\cos(2\phi)$. Here, for the temperature dependence of the gap function, we adopt the well-established α model, i.e., $\Delta(\phi, T) = \alpha\Delta_{\mathrm{BCS}}(\phi, T)$ [42], where $\Delta_{\mathrm{BCS}}(\phi, T)$ is the weak-coupling BCS gap function. This means that we assume a BCS-like gap and use the parameter α to evaluate the strength of electron-phonon coupling. In case of a two-gap fit, two sets of γ_n and α values were used.

At a first glance, all models seem to fit the data well. However, upon magnifying the low-T region [see Fig. 4(b)], one observes clear differences. Thus, neither the single s-wave nor the d-wave model can fit the data satisfactorily. Conversely, a two-gap s-wave model provides an almost ideal fit. For all cases, the corresponding fit parameters are listed in Table I. The resulting $\Delta C/\gamma_n T$ for the two-gap model is equal to 1.3, very close to the weak-coupling BCS value of 1.43. The resultant α values in the two-gap fit suggest the weak-coupling nature of the superconductivity herein.

Figure 5 illustrates the DFT-calculated band structure of TaOsSi. When the SOC is ignored, four bands, arising mainly from the Ta and Os d orbitals, are found to cross the Fermi level E_F. These bands remain at least twofold degenerate at the high-symmetry lines on the Brillouin zone (BZ) boundary. Interestingly, two distinct hourglass band crossings show up between T and Y, and at the S point near the Fermi level E_F. The resulting Dirac points are fourfold degenerate with a linear energy dispersion along all three principal momentum directions. When SOC is accounted for, the number of bands doubles due to the lifting of the degeneracy. Despite the presence of gapped band crossings at the Dirac points, we find that the band structure still crosses the Fermi level. This means that the spin-orbit coupling effects are not strong enough to change the metallic character of TaOsSi.

TABLE I. Fit parameters obtained by using different models of SC pairing symmetry [see Fig. 4(b)].

Pairing	T_c (K)	α	γ_n (mJ mol^{-1} K^{-2})
One s wave	5.95	1	8.5
One d wave	5.85	1.25	9
Two s waves	5.95	(0.3, 1.06)	(1.5, 7.3)

The first BZ, including its high-symmetry points and the full three-dimensional (3D) Fermi surfaces (with color-coded Fermi velocities) are shown in Figs. 6(a) and 6(b), respectively. To further clarify the band-structure of TaOsSi, we calculated also its bulk Fermi surfaces at the $k_x = 0$ plane and the surface-state spectra at a (100) section, as shown in Figs. 6(c) and 6(d), respectively. In the latter case, we clearly observe the appearance of extra surface states (bright red lines), which connect the bulk states. The 3D Fermi surfaces show complex three-dimensional characteristics.

To further confirm the topological nature of TaOsSi, we calculated the Z_2 topological indices (ν_0, $\nu_1\nu_2\nu_3$) normally used to classify the topological band insulators and semimetals [43]. Each of the four invariants takes a value of either 0 or 1, thus enumerating 16 phases belonging to three classes. A nonzero ν_0 indicates that the system is a strong topological insulator (STI). When $\nu_0 = 0$, the systems are further classified according to ν_1, ν_2, and ν_3. Systems with $\nu_1 \neq 0$, $\nu_2 \neq 0$, and $\nu_3 \neq 0$ are called weak topological insulators (WTIs), while the (0, 000) system is a normal insulator (NI). This classification is also appropriate for our case. The Z_2 topological number for a 3D bulk system can be obtained by

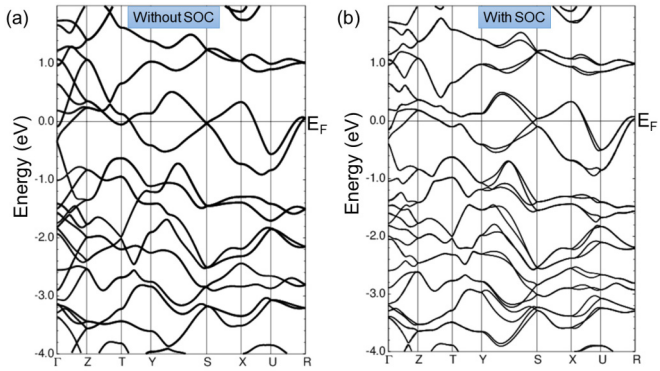

FIG. 5. Electronic band-structure calculations for TaOsSi (a) without accounting for SOC and (b) including SOC.

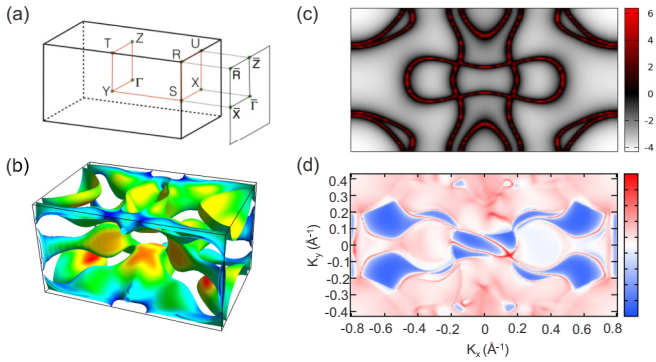

FIG. 6. (a) Bulk and surface first Brillouin zone, illustrating the high-symmetry points. (b) 3D bulk Fermi surfaces and color-coded Fermi velocities (blue is low velocity). (c) Calculated Fermi surfaces at the $k_x = 0$ plane. (d) Surface-state spectra at a (100) section; bright red lines denote surface states.

calculating the Wilson loop for the six time-reversal-invariant momentum planes: $k_x = 0, \pi$; $k_y = 0, \pi$; and $k_z = 0, \pi$. For TaOsSi the Z_2 invariant numbers are 1 for the $k_x = \pi$; $k_y = 0, \pi$; and $k_z = \pi$ planes, and 0 for the other planes. The resulting topological index is (0, 111), which indicates that TaOsSi is a *weak topological material* in all three reciprocal-lattice directions. Unlike "strong" topological insulators, which in an ARPES experiment exhibit large gaps at high-symmetry points, as a "weak" TI, TaOsSi is expected to show additional topological surface states (TSSs) [44].

Besides investigating TaOsSi in standard conditions, we studied some of its properties also under applied pressure, the latter representing a clean way to tune the material properties. The effects of pressure on topological materials have already been studied in several cases [45–48]. For instance, the topological insulator Bi_2Se_3 displays a superconducting and, successively, a structural phase transition under applied pressure. In our case, we studied the pressure effect on the TaOsSi resistivity. Figure 7(a) shows the temperature dependence of resistivity at different pressures, from nearly ambient pressure up to 50 GPa. With increasing pressure, drastic changes are observed in the normal-state resistivity, especially in the 0–5 GPa range. Also, the superconducting transition changes, first by gradually decreasing (for $p \lesssim 26$ GPa) and then by increasing slightly, as the pressure continues to increase [Fig. 7(a), inset]. The pressure-dependent superconducting transition temperature $T_c(p)$ is shown in Fig. 7(b). The observed "V-shaped" dependence of T_c might be due to possible phase transitions across the investigated pressure range.

IV. CONCLUSION

In summary, we studied the upper critical field, the superconducting gap, the band structure, and the pressure effects on the recently discovered TaOsSi superconductor ($T_c \approx 5.8$ K). The upward behavior of its $H_{c2}(T)$ curve implies a multiband superconductivity, further confirmed by calorimetric studies, which indeed indicate the existence of two superconducting gaps. Both gaps, $\Delta_1 = 0.53 k_B T_c$ and $\Delta_2 = 1.87 k_B T_c$, are compatible with the weak-coupling BCS limit. More intriguingly, first-principles DFT calculations indicate the existence

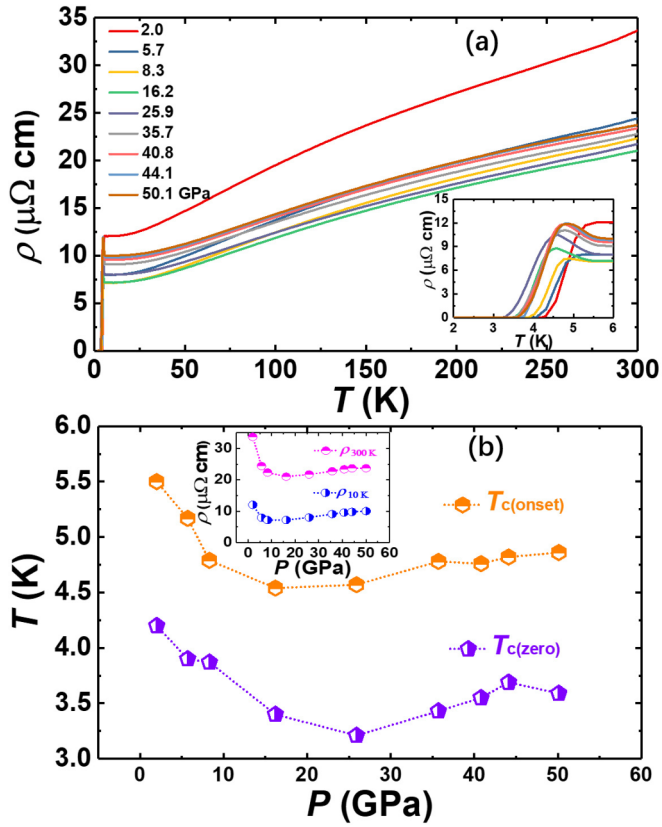

FIG. 7. (a) Temperature-dependent resistivity for different applied pressures. The inset is an enlarged view near the superconducting transition. (b) Pressure dependence of the superconducting transition temperature. T_c(onset) and T_c(zero) refer to the onset of SC transition and to the zero-resistivity SC transition temperature, respectively. The inset shows the resistivity vs pressure, measured at 10 and 300 K.

of Dirac points and topological surface states. These results suggest that TaOsSi is a system where multiband superconductivity coexists with topological surface states, which quite resembles the case in S-doped $MoTe_2$ [49]. In $MoTe_{2-x}S_x$, a clearly larger gap than the bulk superconducting gaps was observed on the sample surface. Whether the large gap results from the interaction between the multigap superconductivity and topological surface states is still a open question. Further theoretical and experimental studies are needed. Nevertheless, similar to $MoTe_{2-x}S_x$, TaOsSi may also provide a new platform in the search for topological superconductors or Majorana fermions. Future local-probe experiments are expected to shed more light on the interesting properties of TaOsSi.

ACKNOWLEDGMENTS

This work was sponsored by the National Natural Science Foundation of China (Grants No. U1732162, No. 11504182, No. 11704047, No. U1832147, No. U1932217, No. 11504329, No. 11674054, and No. 11974061), the Strategic Priority Research Program (B) of the Chinese Academy of Sciences (Grant No. XDB25000000) and the National Key R&D Program of China (Grant No. 2018YFA0704300).

T.S. was in part supported by the Swiss National Science Foundation under Grant No. 200021-169455.

C.Q. Xu, B. Li, and J.J. Feng contributed equally to this work.

[1] M. Sato and Y. Ando, Topological superconductors: A review, Rep. Prog. Phys. **80**, 7 (2017).

[2] M. Leignse and K. Flensberg, Introduction to topological superconductivity and Majorana Fermions, Semicond. Sci. Technol. **27**, 124003 (2012).

[3] X-L. Qi and S-C. Zhang, Topological insulators and superconductors, Rev. Mod. Phys. **83**, 1057 (2011).

[4] M. Z. Hasan and C. L. Kane, Topological insulators, Rev. Mod. Phys. **82**, 3045 (2010).

[5] A. Y. Kitaev, Unpaired Majorana Fermions in quantum wires, Phys. Usp. **44**, 131 (2001).

[6] C. W. J. Beenakker, Search for Majorana Fermions in superconductors, Annu. Rev. Condens. Matter Phys. **4**, 113 (2013).

[7] N. Read and D. Green, Paired states of Fermions in two dimensions with breaking of parity and time-reversal symmetries and the fractional quantum Hall effect, Phys. Rev. B **61**, 10267 (2000).

[8] P. Hosur, P. Ghaemi, R. S. K. Mong, and A. Vishwanath, Majorana Modes at the Ends of Superconductor Vortices in Doped Topological Insulators, Phys. Rev. Lett. **107**, 097001 (2011).

[9] L. Fu and C. L. Kane, Superconducting Proximity Effect and Majorana Fermions at the Surface of a Topological Insulator, Phys. Rev. Lett. **100**, 096407 (2008).

[10] A. Pustogow, Y. Luo, A. Chronister, Y.-S. Su, D. A. Sokolov, F. Jerzembeck, A. P. Mackenzie, C. W. Hicks, N. Kikugawa, S. Raghu, E. D. Bauer, and S. E. Brown, Constraints on the superconducting order parameter Sr_2RuO_4 from oxygen-17 nuclear magnetic resonance, Nature (London) **574**, 72 (2019).

[11] A. P. Mackenzie and Y. Maeno, The superconductivity of Sr_2RuO_4 and the physics of spin-triplet pairing, Rev. Mod. Phys. **75**, 657 (2003).

[12] Y. Ueno, A. Yamakage, Y. Tanaka, and M. Sato, Symmetry-Protected Majorana Fermions in Topological Crystalline Superconductors: Theory and Application to Sr_2RuO_4, Phys. Rev. Lett. **111**, 087002 (2013).

[13] Y. Imai, K. Wakabayashi, and M. Sigrist, Topological and edge state properties of a three-band model for Sr_2RuO_4, Phys. Rev. B **88**, 144503 (2013).

[14] K. Matano, M. Kriener, K. Segawa, Y. Ando, and G.-q. Zheng, Spin-rotation symmetry breaking in the superconducting state of $Cu_xBi_2Se_3$, Nat. Phys. **12**, 852 (2016).

[15] P. Das, Y. Suzuki, M. Tachiki, and K. Kadowaki, Spin-triplet vortex state in the topological superconductor $Cu_xBi_2Se_3$, Phys. Rev. B **83**, 220513(R) (2011).

[16] L. Fu, and E. Berg, Odd-Parity Topological Superconductors: Theory and Application to $Cu_xBi_2Se_3$, Phys. Rev. Lett. **105**, 097001 (2010).

[17] M. Nishiyama, Y. Inada, and G.-q. Zheng, Spin Triplet Superconducting State due to Broken Inversion Symmetry in Li_2Pt_3B, Phys. Rev. Lett. **98**, 047002 (2007).

[18] S. Harada, J. J. Zhou, Y. G. Yao, Y. Inada, and G.-q. Zheng, Abrupt enhancement of noncentrosymmetry and appearance of a spin-triplet superconducting state in $Li_2(Pd_{1-x}Pt_x)_3B$ beyond $x = 0.8$, Phys. Rev. B **86**, 220502(R) (2012).

[19] S. Y. Guan, P. J. Chen, M. W. Chu, R. Sankar, F. C. Chou, H. T. Jeng, C. S. Chang, and T. M. Chuang, Superconducting topological surface states in the noncentrosymmetric bulk superconductor $PbTaSe_2$, Sci. Adv. **2**, e1600894 (2016).

[20] T. R. Chang, P. J. Chen, G. Bian, S. M. Huang, H. Zheng, T. Neupert, R. Sankar, S. Y. Xu, I. Belopolski, G. Q. Chang, B. Wang, F. C. Chou, A. Bansil, H. T. Jeng, H. Lin, and M. Z. Hasan, Topological Dirac surface states and superconducting pairing correlations in $PbTaSe_2$, Phys. Rev. B **93**, 245130 (2016).

[21] M. Sakano, K. Okawa, M. Kanou, H. Sanjo, T. Okuda, T. Sasagawa, and K. Ishizaka, Topologically protected surface states in a centrosymmetric superconductor β-$PdBi_2$, Nat. Commun. **6**, 8595 (2015).

[22] P. K. Biswas, D. G. Mazzone, R. Sibille, E. Pomjakushina, K. Conder, H. Luetkens, C. Baines, J. L. Gavilano, M. Kenzelmann, A. Amato, and E. Morenzoni, Fully gapped superconductivity in the topological superconductor β-$PdBi_2$, Phys. Rev. B **93**, 220504(R) (2016).

[23] H. Xiao, T. Hu, W. Liu, Y. L. Zhu, P. G. Li, G. Mu, J. Su, K. Li, and Z. Q. Mao, Superconductivity in the half-Heusler compound TbPdBi, Phys. Rev. B **97**, 224511 (2018).

[24] O. Pavlosiuk, D. Kaczorowski, and P. Wisniewski, Shubnikov-de Haas oscillations, weak antilocalization effect and large linear magnetoresistance in the putative topological superconductor LuPdBi, Sci. Rep. **5**, 9158 (2015).

[25] C. Liu, Y. Lee, T. Kondo, E. D. Mun, M. Caudle, B. N. Harmon, Sergey L. Bud'ko, P. C. Canfield, and A. Kaminski, Metallic surface electronic state in half-Heusler compounds *R*PtBi ($R =$ Lu, Dy, Gd), Phys. Rev. B **83**, 205133 (2011).

[26] C. Benndorf, L. Heletta, G. Heymann, H. Huppertz, H. Eckert, and R. Pottgen, NbOsSi and TaOsSi — Two new superconducting ternary osmium silicides, Solid State Sci. **68**, 32 (2017).

[27] P. Blaha, K. Schwarz, G. Madsen, D. Kvasnicka, and J. Luitz, WIEN2K, *An Augmented Plane Wave Plus Local Orbital Program for Calculating Crystal Properties* (Vienna, University of Technology, Vienna, 2001).

[28] J. P. Perdew, K. Burke, and M. Ernzerhof, Generalized Gradient Approximation Made Simple, Phys. Rev. Lett. **77**, 3865 (1996).

[29] A. A. Mostofi, J. R. Yates, G. Pizzi, Y. S. Lee, I. Souza, D. Vanderbilt, and N. Marzari, An updated version of WANNIER90: A tool for obtaining maximally-localised Wannier functions, Comput. Phys. Commun. **185**, 2309 (2014).

[30] Q. S. Wu, S. N. Zhang, H. F. Song, M. Troyer, and A. A. Soluyanov, WannierTools: An open-source software package for novel topological materials, Comput. Phys. Commun. **224**, 405 (2018).

[31] X. Lin, B. Fauqué, and K. Behnia, Scalable T^2 resistivity in a small single-component Fermi surface, Science **349**, 945 (2015).

[32] E. Haque and M. A. Hossain, Elastic, electronic, thermodynamic and transport properties of XOsSi ($X =$ Nb, Ta)

superconductor: First-principles calculations, J. Alloys Compd. **739**, 737 (2018).

[33] A. C. Jacko, J. O. Fjarestad, and B. J. Powell, A unified explanation of the Kadowaki-Woods ratio in strongly correlated metals, Nat. Phys. **5**, 422 (2009).

[34] C. Q. Xu, W. Zhou, R. Sankar, X. Z. Xing, Z. X. Shi, Z. D. Han, B. Qian, J. H. Wang, Z. W. Zhu, J. L. Zhang, A. F. Bangura, N. E. Hussey, and X. F. Xu, Enhanced electron correlations in the binary stannide $PdSn_4$: A homologue of the Dirac nodal arc semimetal $PtSn_4$, Phys. Rev. Mater. **1**, 064201 (2017).

[35] O. F. de Lima, R. A. Ribeiro, M. A. Avila, C. A. Cardoso, and A. A. Coelho, Anisotropic Superconducting Properties of Aligned MgB_2 Crystallites, Phys. Rev. Lett. **86**, 5974 (2001).

[36] F. Hunte, J. Jaroszynski, A. Gurevich, D. C. Larbalestier, R. Jin, A. S. Sefat, M. A. McGuire, B. C. Sales, D. K. Christen, and D. Mandrus, Two-band superconductivity in $LaFeAsO_{0.89}F_{0.11}$ at very high magnetic fields, Nature (London) **453**, 903 (2008).

[37] X. Z. Xing, W. Zhou, J. H. Wang, Z. W. Zhu, Y. F. Zhang, N. Zhou, B. Qian, X. F. Xu, and Z. X. Shi, Two-band and Pauli-limiting effects on the upper critical field of 112-type iron pnictide superconductors, Sci. Rep. **7**, 45943 (2017).

[38] J. R. Wang, X. F. Xu, N. Zhou, L. Li, X. Z. Cao, J. H. Yang, Y. K. Li, C. Cao, J. H. Dai, J. L. Zhang, Z. X. Shi, B. Chen, and Z. H. Yang, Upward Curvature of the Upper Critical Field and the V-Shaped Pressure Dependence of T_c in the Noncentrosymmetric Superconductor $PbTaSe_2$, J. Supercond. Novel Magn. **28**, 3173 (2015).

[39] A. Gurevich, Enhancement of the upper critical field by nonmagnetic impurities in dirty two-gap superconductors, Phys. Rev. B **67**, 184515 (2003).

[40] O. J. Taylor, A. Carrington, and J. A. Schlueter, Specific-Heat Measurements of the Gap Structure of the Organic Superconductors κ-$(ET)_2Cu[N(CN)_2]Br$ and κ-$(ET)_2Cu(NCS)_2$, Phys. Rev. Lett. **99**, 057001 (2007).

[41] X. Xu, B. Chen, W. H. Jiao, B. Chen, C. Q. Niu, Y. K. Li, J. H. Yang, A. F. Bangura, Q. L. Ye, C. Cao, J. H. Dai, G. Cao, and N. E. Hussey, Evidence for two energy gaps and Fermi liquid behavior in the $SrPt_2As_2$ superconductor, Phys. Rev. B **87**, 224507 (2013).

[42] H. Padamsee, J. E. Neighbor, and C. A. Shiffman, Quasiparticle phenomenology for thermodynamics of strong-coupling superconductors, J. Low Temp. Phys. **12**, 387 (1973).

[43] L. Fu and C. L. Kane, Topological insulators with inversion symmetry, Phys. Rev. B **76**, 045302 (2007).

[44] R. Noguchi, T. Takahashi, K. Kuroda, M. Ochi, T. Shirasawa, M. Sakano, C. Bareille, M. Nakayama, M. D. Watson, K. Yaji, A. Harasawa, H. Iwasawa, P. Dudin, T. K. Kim, M. Hoesch, V. Kandyba, A. Giampietri, A. Barinov, S. Shin, R. Arita, T. Sasagawa and T. Kondo, A weak topological insulator state in quasi-one-dimensional bismuth iodide, Nature (London) **566**, 518 (2019).

[45] P. P. Kong, J. L. Zhang, S. J. Zhang, J. Zhu, Q. Q. Liu, R. C. Yu, Z. Fang, C. Q. Jin, W. G. Yang, X. H. Yu, J. L. Zhu, and Y. S. Zhao, Superconductivity of the topological insulator Bi_2Se_3 at high pressure, J. Phys.: Condens. Matter **25**, 362204 (2013).

[46] C. Q. Xu, B. Li, M. R. van Delft, W. H. Jiao, W. Zhou, B. Qian, Nikolai D. Zhigadlo, Dong Qian, R. Sankar, N. E. Hussey, and Xiaofeng Xu, Extreme magnetoresistance and pressure-induced superconductivity in the topological semimetal candidate YBi, Phys. Rev. B **99**, 024110 (2019).

[47] Y. Qi, W. J. Shi, P. Werner, P. G. Naumov, W. Schnelle, L. Wang, K. G. Rana, S. Parkin, S. Medvedev, B. Yan, and C. Felser, Pressure-induced superconductivity and topological quantum phase transitions in a quasi-one-dimensional topological insulator: Bi_4I_4, npj Quantum Mater. **3**, 1 (2018).

[48] Y. T. Chan, P. L. Alireza, K. Y. Yip, Q. Niu, K. T. Lai, and S. K. Goh, Nearly isotropic superconductivity in the layered Weyl semimetal WTe_2 at 98.5 kbar, Phys. Rev. B **96**, 180504(R) (2017).

[49] Y. Li, Q. Gu, C. Chen, J. Zhang, Q. Liu, X. Hu, J. Liu, Y. Liu, L. Li, M. Tian, Y. Wang, N. Samarth, S. Li, T. Zhang, J. Feng, and J. Wang, Nontrivial superconductivity in topological $MoTe_{2-x}S_x$ crystals, Proc. Natl. Acad. Sci. USA **115**, 9503 (2018).